Parameter-space studies of Dark Matter annihilations in the Sun in the scotogenic minimal model

Bachelor Thesis
by
Tim Kopka

- June 2021 -

AG Kappes
Institute of Nuclear Physics
Westfälische Wilhelms-Universität Münster

Supervisor: Prof. Dr. Alexander Kappes
Second examiner: Prof. Dr. Christian Weinheimer

This Bachelor thesis was undertaken in the working group of Prof. Dr. Kappes, WWU Münster.

Contents

Introduction

1

The advances of particle physics in the last few decades have led to a very detailed description of the elementary particles in our universe, put together in the *Standard Model* (SM). However, while its success (e.g. in predicting experimental outcomes) is indisputable in many ways, scientists are still searching for physics beyond the Standard Model. An increasing amount of astronomical observations hint at a substantial amount of non-visible matter, which cannot be measured directly, and is therefore known as *Dark Matter* (DM). It is not explained by the Standard Model, and is hence probably the biggest puzzle that fascinates modern physicists. Despite a large amount of ongoing research and experimental searches, no one has been able to measure and show its nature yet. At the same time, various theoretical models are being proposed and studied in order to get an idea of what Dark Matter could be, and to understand possible experimental evidence that could confirm these models in the future.
A popular approach for a Dark Matter candidate is the *weakly interacting massive particle* (WIMP). It is hypothesised to interact via gravity and the weak force and could present a solution to the missing mass problem. This work focuses on the *scotogenic minimal model*, which provides a WIMP Dark Matter candidate particle and gives a solution to the neutrino mass problem of the Standard Model. Its parameter-space, as well as a comparison to experimental constraints, are described in the course of this work. Additionally, Dark Matter annihilation processes in the Sun, which are crucial for indirect Dark Matter detection, are studied and outlined.
For better comprehension, abbreviations and symbols are listed in table 1.1. Also note the difference between the known and experimentally measured particles of the Standard Model (SM) and the unknown hypothetical particles provided by the Dark Matter model (DM). This work is a Bachelor's thesis in physics, therefore detailed formula and descriptions will not be given and the reader is referred to the relevant literature. Instead, the focus is laid on basic understanding and phenomenology.
First, a theoretical summary of the concepts needed for this work is given, followed by a description of the numerical analysis tool-chain. After a brief explanation of relevant Dark Matter experiments and constraints, the results of multiple parameter scans are presented and discussed.

Table 1.1: Overview of abbreviations and symbols used in this work.

Abbreviation / Symbol	Explanation	See
BSM	Beyond the Standard Model	section 2.2
CDM	Cold Dark Matter	section 2.2
CMB	Cosmic Microwave Background	section 2.2
DM	Dark Matter	section 2.2
EWSB	Electro Weak Symmetry Braking	section 2.1
IC86	IceCube Experiment (with 86 strings)	chapter 4
PMT	PhotoMultiplier Tube	chapter 4
SM	Standard Model	section 2.1
VEV / $\langle \phi^0 \rangle$	Vacuum Expectation Value (of the SM Higgs field)	section 2.3
WIMP / χ	Weakly Interacting Massive Particle	section 2.2
ν	Neutrino	section 2.1

Theory

2

In this chapter, the background of this work will be studied in detail. First, the current knowledge of elementary particles is outlined, followed by a description of limitations that motivate physicists for a search beyond the Standard Model. Subsequently, the scotogenic model and its parameters are presented. Finally, capturing and annihilation processes of Dark Matter are explained and applied on the Sun.

2.1 The Standard Model

When studying modern particle physics, it is impossible to avoid working with the Standard Model (SM). This theory provides the fundamental building-blocks of the universe that are known so far. The general outline as well as some features relevant to this work are explained in the following.
The elementary particles which are included in the Standard Model consist of two groups: *Fermions* and *bosons* (see white and coloured boxes respectively in fig. 2.1). Fermions are the particles that make up most of the normal matter (predominantly in the form of atoms), while bosons (e.g. gluons, photons) generally work as force mediators (the forces and their mediators are shown by colors in fig. 2.1). Further differences between these two groups can also be found in their statistical distributions and spin values. Furthermore, fermions also have respective anti-particles with opposite charges.
Regarding the bosons, the Higgs-boson has a special role. It was theoretically predicted in the 1960s and only discovered in 2012 at the LHC at CERN [2]. As mediator of the Higgs-field, the boson interacts with all particles that carry mass. It also fills an important role in *electroweak symmetry breaking* (EWSB) by inducing the Higgs mechanism, a process through which the weak gauge bosons obtain their masses.
The Standard Model is a well tested theory and provides explanations for many phenomena. For example, many processes predicted by the SM could be largely confirmed by measurements at the LHC.
In the following, two aspects of the Standard Model which are important for this work will be described into more detail.

Theoretical formulation

The Standard Model is a *Quantum Field Theory* that describes particles as exitations of quantum fields. The interactions and properties of these fields are denoted in the *Lagrangian* $\mathcal{L}$ (which is qualitatively well explained in [3]).
As this is the basis of the Standard Model, every extension to the SM has to contribute to the Lagrangian. Fortunately, in the frame of the mathematical description, this can be done by simply adding additional terms which are denoted by $\mathcal{L}_N$. The theoretical addition to the Lagrangian of the scotogenic model (which is studied in this work) will be described in section 2.3.

Neutrinos

The three neutrino particles (lower left in fig. 2.1) are a relatively recent discovery (even though Wolfgang Pauli already postulated them in the 1930s). In 1956, the electron-neutrino ν_e was measured by F. Reines and C. Cowan [4], followed by the

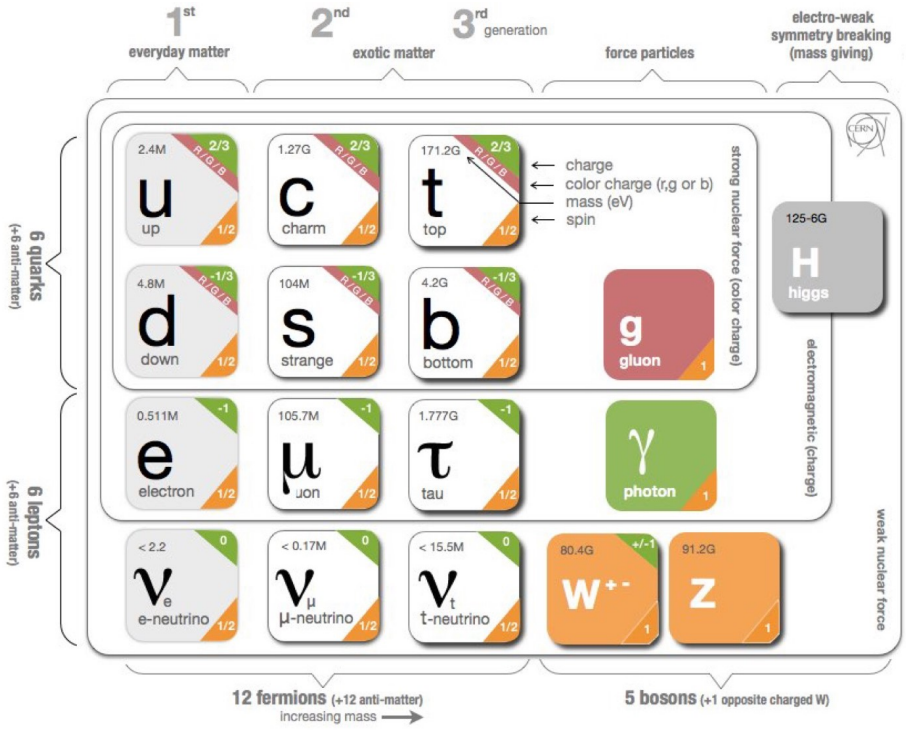

Figure 2.1: Overview of the particles included in the Standard Model (SM). On the left side, the 12 fermions are shown, with their respective charges and masses in the corners including the three neutrinos in the lowest row. On the right side, the five bosons are depicted, which include the most recently discovered SM Higgs Boson. Figure adapted from [1].

muon-neutrino ν_μ 1962 at the Brookhaven Particle Accelerator [5], and, finally, the tau-neutrino ν_τ in 2001 [6]. One reason for their late discovery is their mode of interaction: Neutrinos only couple weakly, hence to W and Z bosons[1].

In the Standard Model, neutrinos are expected to be massless [7]. However, neutrino oscillations have been detected experimentally, which means that the particles change/oscillate between their *flavours e, μ* and τ while travelling through space and time. This led to the conclusion that neutrino states with distinct masses have to exist, which contradicts the SM prediction [7].

This is a phenomenon which has left many physicists wondering, and is subject to modern research, both experimentally and theoretically. Currently, multiple experiments are trying to determine the values of the masses and their order which is called *neutrino hierarchy*. On the theoretical side, possible possible extensions to the Standard Model are suggested. The model which is studied in this work also provides an explanation for the neutrino masses.

Because Neutrinos don't carry electrical charge and only interact weakly, they are hard to measure in physical detectors. One approach is to use large volumes and to exploit natural materials such as ice: The IceCube Neutrino Observatory is placed at the South Pole, and consists of many sensors which are placed underground in the ice.

[1]Neutrinos also interact via gravity. However, this force is commonly neglected as their mass is extremely small.

They detect the Cherenkov light, which is produced as a result of neutrinos travelling through the ice (for further description of the experiment see chapter 4).

2.2 Beyond the Standard Model: Dark Matter

As mentioned earlier, the Standard Model of Particle Physics is thoroughly tested and its predictions are backed up by many experiments (e.g. at the Large Hadron Collider at CERN). However, for more than eight decades, astronomical observations provided evidence for *Beyond the Standard Model* (BSM) physics. For instance, stellar objects don't move as they are expected to (described in [8]), which is hinting to more mass in the universe than is visible.

One example was found by Fritz Zwicky in the 1930s [9]: He studied the Coma cluster, which is a gravitationally stable galaxy cluster. He applied the *virial theorem* to the velocities of the galaxies, which connects the average kinetic energy of a stable system to its potential energy. Hence by studying the velocities of the galaxies, he was able to predict the gravitational potential of the whole cluster. Additionally, he calculated the mass of the visible stars from their measured light. These two methods returned contradicting results: Much more (non visible) mass is needed than the known mass of all observed stars combined, which Zwicky called "Dunkle Materie" (*Dark Matter*) [10]. This discrepancy between visible and non visible mass has been confirmed again with more accurate data since then (e.g. in [11]), and was also found in many other astronomical systems.

While studying the universe, hints for this Dark Matter were also found in the Cosmic Microwave Background (CMB) [12]. This radiation can be measured in all directions from Earth, and makes it possible to infer the matter distribution in the early universe. The fluctuations which can be observed (e.g. that galaxies and galaxy clusters exist), cannot be explained only by baryonic (Standard Model) matter, but other particles are needed [10]. By studying the Cosmic Microwave Background (see chapter 4), the amount of the Dark Matter that still exists today can be calculated using cosmological models. This is referred to as *relic density*.

If Dark Matter particles are assumed to exist, how could these particles interact (additionally to gravity via mass)? If electromagnetic or via the strong force, it is commonly expected that signals already would have been detected. The weak force remains as a possible mode of interaction. This type of Dark Matter is therefore referred to as *weakly interacting massive particles* (WIMPs, often denoted by the Greek letter χ) and presents one of the most popular approaches to the Dark Matter problem. Alternative hypotheses exist, for instance *axions* or *massive compact halo objects* [10]. There are various searches for Dark Matter WIMPs currently ongoing, and general principles as well as a few experiments will be described in chapter 4.

The theoretical model studied in this work proposes WIMP Dark Matter. It is called the *scotogenic minimal dark matter model* or short *scotogenic*. The term *minimal* refers to the fact that only a handful particles are added to the Standard Model to account for Dark Matter, which contrasts to other popular theories such as the *supersymmetry* theory.

2.3 The scotogenic minimal model

One specific minimal model scenario was originally proposed in 2006 by Ernest Ma as *Radiative Seesaw Model* [13] and is now often referred to as the *Scotogenic Model*[2]. Two core features of the model are especially important:

1. The model introduces stable WIMPs: A new symmetry called Z_2 is implemented in which the newly added particles are defined to be odd. In contrast to this, the Standard Model matter is set to be even under the Z_2-symmetry. The odd particles can decay inside the odd sector, leaving the lightest odd particle stable, which therefore is the Dark Matter WIMP candidate.

2. In the scotogenic model, the neutrinos can obtain masses: As a direct consequence of this new Z_2-symmetry, the neutrinos can interact with the Higgs field via the new added Dark Matter particles (this is happening in a next-level order Feynman diagram, see fig. 2.2). Through this coupling, which is forbidden within the SM, the neutrinos obtain their masses. This is called the *radiative seesaw mechanism* (which was the motivation for the original name of the model).

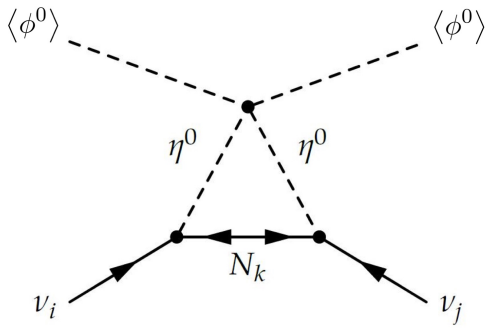

Figure 2.2: Feynman diagram of how SM neutrino masses are generated by the *radiative seesaw mechanism*. $\langle\phi^0\rangle$ is the SM Higgs *vacuum expectation value* (VEV), η^0 and N_k denote the new DM particles and ν_i are the SM neutrinos. Further explanations can be found in [14], [15]. Credit: [14], *p.102*.

A more detailed description of the scotogenic model is given hereafter. However, the most important aspects (for this work) are summarised at the end of this subsection. The basic ingredients are the following new added particles: A scalar doublet η, which couples to the Higgs boson and therefore also is subject to electro-weak symmetry breaking (EWSB). And three generations of fermion singlets N_i (sort of "right-handed neutrinos"). These function as the heavy counterparts of the Standard Model neutrinos.
Mathematically, the scotogenic model introduces the new Lagrangian (from [15])

$$\mathcal{L}_N = -\frac{m_{N_i}}{2} N_i N_i + y_{i\alpha} \left(\eta^\dagger L_\alpha\right) N_i + \text{ h.c. } - V, \tag{2.1}$$

which includes the Yukawa-coupling $y_{i\alpha}$, the SM leptons L_α ($\alpha = 1, 2, 3$) and the

[2]Scotogenic from Greek, can be translated with "created from darkness".

fermionic masses m_{N_i}. The potential is

$$V = m_\phi^2 \phi^\dagger \phi + m_\eta^2 \eta^\dagger \eta + \frac{\lambda_1}{2}\left(\phi^\dagger \phi\right)^2 + \frac{\lambda_2}{2}\left(\eta^\dagger \eta\right)^2 + \lambda_3 \left(\phi^\dagger \phi\right) \left(\eta^\dagger \eta\right) + \lambda_4 \left(\phi^\dagger \eta\right)\left(\eta^\dagger \phi\right) + \frac{\lambda_5}{2}\left[\left(\phi^\dagger \eta\right)^2 + \left(\eta^\dagger \phi\right)^2\right], \tag{2.2}$$

with the Higgs field ϕ and the squared mass input parameter m_η^2. λ_1 and m_ϕ are fixed by the Higgs *vacuum expectation value* $\langle \phi^0 \rangle$ and the (squared) SM Higgs boson mass m_h^2 which have been measured [2]. Hence $\lambda_1 = 0.26$ and $m_\phi^2 = -0.5 m_h^2$ [15]. In this work, λ_2 is set to 0.5 without loss of generality [15]. The other parameters λ_3, λ_4 and λ_5 are described in the next section.
Because of EWSB, the Dark Matter field η splits up into a positive η^+ and a neutral component $\eta^0 = \left(\eta^{0R} + i\eta^{0I}\right)/\sqrt{2}$. The physical particles therefore obtain their masses depending on the λ-parameters and $\langle \phi^0 \rangle$ [15]:

$$m_{\eta^+}^2 = m_\eta^2 + \lambda_3 \left\langle \phi^0 \right\rangle^2 \tag{2.3}$$

$$m_{\eta^{0R}}^2 = m_\eta^2 + (\lambda_3 + \lambda_4 + \lambda_5) \left\langle \phi^0 \right\rangle^2 \tag{2.4}$$

$$m_{\eta^{0I}}^2 = m_\eta^2 + (\lambda_3 + \lambda_4 - \lambda_5) \left\langle \phi^0 \right\rangle^2 \tag{2.5}$$

Note that the mass difference between the two neutral components is only dependent on λ_5, which makes it an important parameter in the scotogenic model (combine eqs. (2.4) and (2.5): $m_{\eta^{0R}}^2 - m_{\eta^{0I}}^2 = \lambda_5 \langle \phi^0 \rangle^2$). Furthermore, the masses of the DM fermions are m_{N_i} as described above.
The Dark Matter candidate is the lightest of the newly introduced particles, if it is uncharged, because the heavier Dark Matter particles decay. As a direct result of the global symmetry, because it cannot decay further into Standard Model particles, this stable DM candidate remains.
The phenomenology of the scotogenic model can manifest in two different scenarios:

Scalar scenario: $m_{\eta^{0R}}$ or $m_{\eta^{0I}}$ is the smallest mass of the particles in the Dark Matter sector, making a scalar particle the DM candidate (studied in sections 5.1 and 5.2). The mass of the charged scalar m_{η^+} could also be the smallest mass, however, this would provide a charged particle as DM candidate, which is not a WIMP and not considered here.

Fermionic scenario: One of the DM fermions N_i has the lightest mass m_{N_i} and serves as the DM candidate (see section 5.4)

In this work, the scalar scenario is mostly put into focus as only this leads to DM capture and annihilation in the Sun (see section 2.5).
Overall, the important point to keep in mind for this work is that there are five different options for the Dark Matter candidate in the scotogenic model (η^{0R}, η^{0I} which lead to a scalar scenario; and N_1, N_2, N_3, which produce a fermionic scenario). For one specific set of parameters, only one of them is the lightest and hence accounts for the expected Dark Matter particle (which also falls into the category as a WIMP, which will be therefore used as a synonym in the course of this work).

2.4 Parameter-space

In the scotogenic model, there are a number of parameters, which can be varied freely within certain bounds. One specific set of parameters is called a *parameter point* that is fully defined and yields a specific set of *observables* for every simulation. Observables are the experimentally measurable values of the model, for example the relic density or the neutrino flux from the Sun. All of the parameter points together form the *parameter-space*.
In this work, the following parameters were changed and sampled depending on the aim of the scan (following [15]):

The parameters λ_3, λ_4 and λ_5 are studied in intervals that still ensure that the scalar potential is bounded from below, and that the vacuum is stable [15]. Additionally, a pertubativity limit of $|\lambda_{2,3,4,5}| < 4\pi$ is required. These intervals are:
$\lambda_3 \in [-\sqrt{\lambda_1\lambda_2}, 4\pi]$,
$\lambda_4 \in [-\sqrt{\lambda_1\lambda_2} - \lambda_3 + |\lambda_5|, 4\pi]$ and
$\lambda_5 \in \pm[10^{-12}, \lambda_3 + \lambda_4 + \sqrt{\lambda_1\lambda_2}]$.
The lower bound for λ_5 is chosen because it is sufficiently small to create effects such as coannihilations between η^{0R} and η^{0I}.

The scalar mass parameter m_η is studied in the range between 10 GeV and 10 TeV because this roughly corresponds to the mass ranges investigatable by the experiments IceCube and XENON (see chapter 4). The masses of the actual scalar particles are dependent on this input as well as the λ-parameters, see eqs. (2.3) to (2.5).

The fermion mass parameters m_{N_1}, m_{N_2} and m_{N_3} are varied in the same range as the scalar mass in the interval [0.01,10] TeV.

Additionally, some constraints are already considered inherently in the setup of the model. One of them is the lowest neutrino mass eigenstate m_{ν_1}, which is randomly sampled in the interval $[4 \times 10^{-3}, 2]$ eV for every parameter point, with the neutrino hierarchy (which determines the order of the neutrino mass differences) set to *normal hierarchy*. The higher mass states m_{ν_2}, m_{ν_3} are then sampled in their uncertainties relative to m_{ν_1} (according to [16], *table 1*).
Secondly, the Yukawa-matrix $y_{i\alpha}$, is based on the neutrino mixing. It occurs in the new Lagrangian (eq. (2.1)) and determines the coupling between the DM fermions, DM scalars and SM particles. This matrix is sampled and calculated according to Casas and Ibarra [17] using data from [18]. The same mechanisms as described in [15] are implemented.
Important for this work is the effect that the Yukawa coupling is calculated based on the set neutrino mass and the parameter λ_5. Hence smaller λ_5 result in bigger Yukawa couplings and the other way around (some effects of this can be seen in section 5.5).
With the here described parameters in mind, this work studies the behaviour of the scotogenic model in response to certain parameter variations. Therefore, multiple scans in the parameter-space were conducted, which are the main subject of this work.

2.5 Dark Matter capture and annihilation

In the frame of the Dark Matter WIMP theory (as explained above), it is assumed that Dark Matter particles have a certain model-dependent abundancy in the universe. As

celestial objects move through space, it is possible that the DM particles are captured by these objects and subsequently annihilate into Standard Model particles. These processes will be explained in detail in the following.

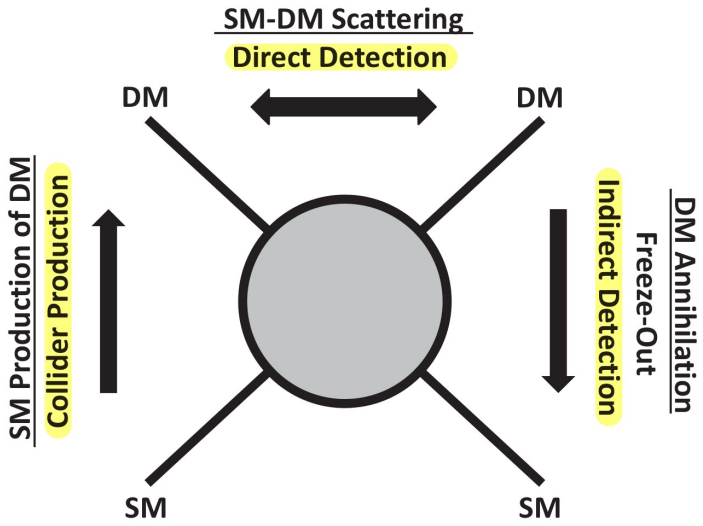

Figure 2.3: Diagram of possible DM-SM particle interactions. The reading direction defines the process (similar to Feynman-diagrams). Highlighted in yellow are the detection methods (see chapter 4). Credit: [19, p. 358]

A celestial object such as the Sun consists of atoms which are mostly defined by their nucleus which is made up of protons and neutrinos (called *nucleons*). For studies with gravity and the weak force, the electrons of the atoms can be neglected because they are significantly lighter than the nucleons (for electromagnetic interactions they are important because of their electric charge).
From measurements of the radial velocities of spiral galaxies, it is assumed that Dark Matter can be found in a so called *halo*, a sphere of Dark Matter particles surrounding the galactic center. This is also expected for the Milky Way. While the Sun is passing through this Dark Matter halo, the Dark Matter particles (here WIMPs) can scatter with the Sun's nucleons. This scattering is schematically displayed horizontally in fig. 2.3. After multiple scattering processes, the Dark Matter particles get captured and follow the path of the Sun. The rate of this *Dark Matter capturing* process is dependent on the *WIMP-nucleon cross-section* which describes the probability of a scattering process. If the cross-section is larger, more Dark Matter particles get captured. The Sun is considered in this work, because it is by far the largest and most massive body in our solar system, which therefore has the highest capture rate.
As this is happening all the time, more and more Dark Matter particles are subject to capturing and a local over-density in the Sun arises. Eventually, if the amount of Dark Matter is high enough, the WIMPs begin to *annihilate* into Standard Model particles. This corresponds to the process shown in fig. 2.3 from top to bottom. These Standard Model particles subsequently interact and decay further into neutrinos which are able to leave the Sun and can be measured on Earth.
In general, the overall scattering happens via elastic ($\chi + nucleon \rightarrow \chi + nucleon$) and inelastic processes. In this work, only elastic scattering in the Sun is taken into account. The consideration of inelastic Dark Matter scattering in the scotogenic model

would go beyond the scope of this thesis, but was studied in [20].

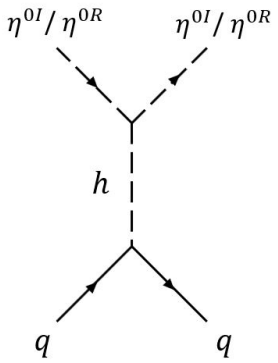

Figure 2.4: Feynman diagram of elastic scattering at nucleons in the scotogenic model in the case of scalar DM with η^{0I} or η^{0R} as lightest DM particle. Here, elastic scattering (spin-independent) happens via the SM Higgs boson h at the SM quarks q (which make up nucleons).

This description is independent of the specific DM model. Looking at the scotogenic model, Dark Matter capture in the Sun happens only in the case of the scalar scenario. The specific diagram for scattering then results in fig. 2.4. Here, the scalar Dark Matter particles scatter via the Higgs boson[3].
In the fermionic case of the scotogenic model, the Dark Matter particle is a fermion singlet and the WIMP-nucleon scattering cross-section is zero. Thus, no capturing and subsequently no annihilation happens in the Sun in this case [20]. Consequently, this work mostly studies the case of scalar DM as this can be compared against the limit by XENON1T and possibly be detected by IceCube (see chapter 4).
The scattering, capture and annihilation processes eventually are expected to lead to a state called *equilibrium*, which will be described further in the following.

Equilibrium in the Sun

The number of accumulated DM particles in the sun can be described mathematically with the differential equation [21]

$$\dot{N}_\chi = C_\chi - A_{\chi\chi} N_\chi^2 - E N_\chi, \tag{2.6}$$

for the DM particle number N_χ with the capture rate C_χ, rate of depletion $A_{\chi\chi}$ and evaporation rate E. The rate of depletion is calculated from

$$A_{\chi\chi} = \frac{\langle \sigma v \rangle_{\chi\chi}}{V_{\text{eff}}}, \tag{2.7}$$

which includes the averaged velocity cross-section of DM annihilation into SM particles $\langle \sigma v \rangle_{\chi\chi}$ and the effective volume of the Sun V_{eff} as described in [21]. Following the paper [21], if the evaporation rate is neglected (see [22]), the solution of eq. (2.6) is the annihilation rate

$$\Gamma_{\chi\chi} = \frac{C_\chi}{2} \tanh^2(\sqrt{C_\chi A_{\chi\chi}} t). \tag{2.8}$$

[3] Z-boson scattering is also possible in the scotogenic model, but this only occurs in the inelastic case. This is covered in [20].

This includes the age of the Sun t, and can be simplified to $\Gamma_{\chi\chi} = \frac{C_\chi}{2}$ if the value which is inserted into the tanh() is large enough (and the hyperbolic tangent squared therefore equals to 1). If this is the case, the state of the Sun is called *equilibrium*.
The capture rate C_χ is therefore the limiting maximum factor of the annihilation rate. This equilibrium always arises at some point in time, however, for small capture rates or even small annihilation rates, this can take very long (and the Sun would not yet have reached this equilibrium).
For experimental purposes, equilibrium between capture and annihilation is desirable because it would generate the highest possible number of annihilations in the Sun. This leads to higher fluxes of particles which can leave the Sun and be measured on Earth (for example neutrinos).
In this work, some aspects of this will be studied (see section 5.3) with regards to the *equilibrium factor* c_{eq}. This is introduced and defined in this thesis as

$$c_{eq} = \tanh^2(\sqrt{C_\chi A_{\chi\chi}}t), \tag{2.9}$$

and equals to 1 in the case of equilibrium.

Numerical analysis tool-chain

3

Simulating the scotogenic model is achieved by using three different programs that were put into a *tool-chain*. The chain and specific input files can be seen in fig. 3.1.

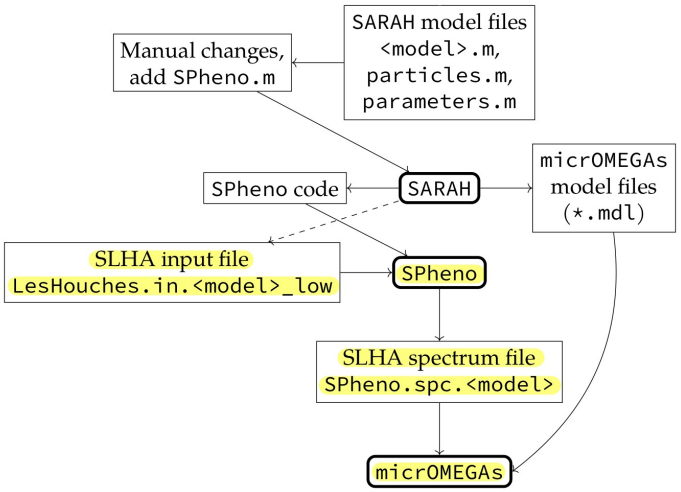

Figure 3.1: Overview of the programs used in this work for the study of the scotogenic model. The steps highlighted in yellow were repeated and adjusted for every parameter point during a parameter scan. Adapted from [14], *fig. 6.1.*

These programs are designed specifically for research about Dark Matter and provide the needed functions:

SARAH (4.14.0) [23]: A Mathematica package for building the environment of the model. Calculates the setup for `SPheno` and the model file for `micrOMEGAs` .

SPheno (4.0.4) [24]: Creates specifications of the model at an exact point and returns a spectrum file as input for `micrOMEGAs`.

micrOMEGAs (5.0.9) [25]: Calculates *observable* and properties of a specific parameter point.

The last program in the chain, `micrOMEGAs`, has various output possibilities including fluxes, decay channels of the DM particles, the relic density, lepton flavour violation processes and (DM) annihilation channels.
For studies of the equilibrium in the Sun (see section 5.3), the built-in function `neutrinoFlux()` is used. It calculates the neutrino flux on Earth from Dark Matter annihilation in the Sun. In order to do this, it solves the differential equation eq. (2.6) numerically. The result was used to determine the *eq factor*.
When changing the parameters from one point to another in the parameter-space, the programs `SPheno` and `micrOMEGAs` have to be run again. This was automated in a *parameter scan* which will be briefly described in the following.

In order to study many points quantitatively, a parameter scan setup was used. The basic functioning of the code was to set up a point randomly according to the set limits, and then executing `SPheno` and `micrOMEGAs` (highlighted in fig. 3.1).

The points were randomly sampled in distributions fitting to their intended scaling: For example λ_5 was sampled with a logarithmic distribution to ensure a similar amount of points for every logarithmic order.
This setup is utilised to study the parameter-space of the scotogenic model in regard to the Lagrangian coupling constants and the masses.

Dark Matter experiments and constraints

4

Following the motivation for Dark Matter as explained in section 2.2, many experiments have since contributed to the search (or are still ongoing, or are planned). A common sketch of the different approaches can be seen in fig. 2.3. This diagram depicts possible interactions of Dark Matter with Standard Model particles. The reading direction defines the exact process, which is either scattering, annihilation or production of DM particles. Experimental setups can focus on these processes and can therefore be placed in fig. 2.3, which is highlighted in yellow.

On the hunt for Dark Matter, experiments search for signals that show different features of the new particles. However, if no Dark Matter signals are measured, it is possible to constrain models and rule out regions of the parameter-space. If a point in a Dark Matter model is not excluded by experimental constraints, it is called *viable*. The experiments and their constraints considered in this work are explained in the following.

Direct detection: XENON1T

One approach is *direct detection* (read fig. 2.3 horizontally). It utilises the scattering of a DM particle with a SM particle, during which the Dark Matter can transfer some energy to the Standard Model particle (in form of recoil energy), which subsequently radiates this energy. The probability of this scattering is described by the *WIMP-nucleon cross-section*, which has a *spin-independent* and a *spin-dependent* part.

In the XENON1T experiment [26], the recoil energy, which is the deposited energy from the Dark Matter to the Standard Model particle, is measured using a tank filled with xenon. It is placed inside a water shield deep underneath a mountain in order to reduce background signals. If a Dark Matter particle scatters of a xenon atom, photons are emitted, which are recorded by *photo-multiplier tubes* (PMTs) that are placed at both ends of the tank. Additionally, electrons that are freed in the process drift through the chamber because of an electric field. When they reach the top of the tank, they produce scintillation light in a gas chamber on top of the liquid xenon. This light then hits the PMTs and gets recorded as a second signal. The combination of the photon and electron signal allows for better background reduction and a spacial resolution of the scattering events in the tank.

No clear WIMP signal has been found in the XENON1T experiment, and the results of the experiment are instead used to constrain the search by setting upper limits to the WIMP-nucleon spin-independent and spin-dependent cross-sections [26]. For direct detection, the spin-independent limits are usually the stronger ones and will be used later in this work (see in fig. 5.2). An upgrade of the XENON1T experiment with a larger volume, called XENONnT, started taking data in 2020 and is expected to set even stronger constraints in the next years [27].

In the scope of the scotogenic model, this detection method only works for the scalar scenarios (η^{0R} or η^{0I}) because the fermion DM particles do not scatter with nuclei.

Reading fig. 2.3 from top to bottom, the operating principle of indirect detection is shown: Two Dark Matter particles annihilate into Standard Model particles, which then can be measured. An advantage is that Dark Matter itself is not needed in the detector and that the experiment can be easier optimised to measure Standard Model particles.
The capture and annihilation of Dark Matter particles happens in large celestial objects as described in section 2.5. The largest object in the Solar System is the Sun, where a local over-density of DM particles is expected in the scalar scenario, which increases the annihilation rate compared to empty space. This access then boosts the neutrino flux from the Sun which therefore is expected to make it possible to investigate on Earth. This flux strongly depends on the main annihilation channels. In this work, the detection of neutrinos in the *IceCube Neutrino Observatory* from DM annihilations in the Sun is calculated and discussed.

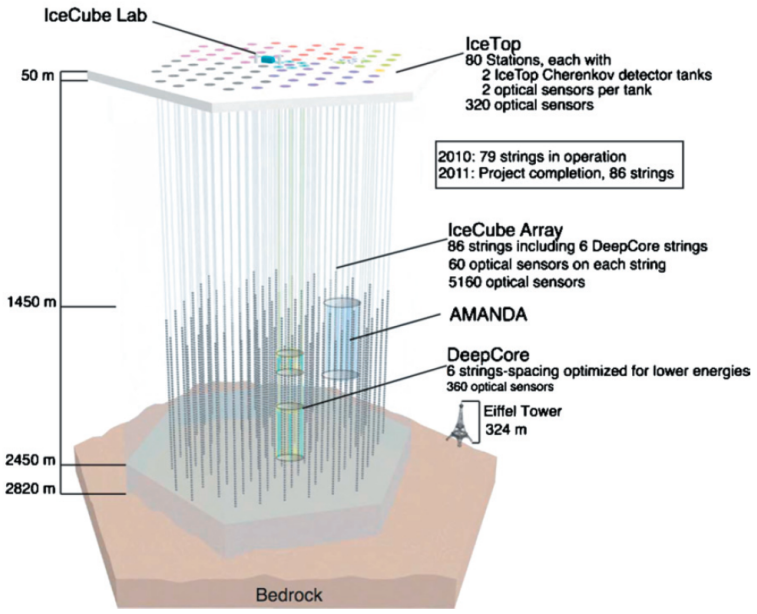

Figure 4.1: Setup of the IceCube Neutrino Observatory in its current form, completed in 2011. It is located next to the *Amundsen-Scott South Pole Station* in Antarctica. [28]

The IceCube experiment is the largest neutrino detector in the world with an instrumented detector volume of 1 km^3, located at the South Pole. The detector consists of 5160 optical modules, each housing a ten-inch photo-multiplier. The modules are attached to 86 strings which are deployed in the ice. A detailed sketch of the setup can be seen in fig. 4.1.
When a neutrino passes the ice, it can scatter of a water atom and produce secondary, charged particles. These can generate Cherenkov light, which is detected by the PMTs. From this it is possible to deduce the energy and also the direction of the neutrinos.
The event rate of neutrinos resulting from Dark Matter annihilation in the Sun is an observable, and can be used in order to study the potential of the scotogenic model to

be measured in the IceCube Neutrino Observatory. This is only possible for the scalar scenario and is also subject in [20].

Planck Space Telescope

The Planck Space Telescope was used to measure the Cosmic Microwave Background (CMB) between 2009 and 2013 with high precision. The telescope measured the CMB fluctuations, from which the collaboration concluded a Dark Matter *relic density* of $\Omega_{\text{CDM}}h^2 = 0.120 \pm 0.001$ [12]. h is the Hubble constant in terms of 100 km s^{-1} Mpc^{-1}. In this work, an interval with 0.02 deviation to the measured value is considered to account for numerical fluctuations and to study trends more easily (following [15]).

Lepton flavour violation processes

In particle physics, interactions between particles obey specific conservation numbers. In the Standard Model, the rates of Lepton Flavour Violation (LFV) processes are very limited. However, the existence of Dark Matter could push the rates of LFV processes and hence parameter points with high lepton flavour violation can be excluded by experimental constraints.
In this work, the expected rate of three experimentally studied processes is considered. The experimental boundaries are

$$\begin{aligned} \text{BR}(\mu \to e\gamma) &< 4.2 \cdot 10^{-13}\,[29], \\ \text{BR}(\mu \to 3e) &< 1.0 \cdot 10^{-12}\,[30], \\ \text{CR}(\mu - e, \text{Ti}) &< 4.3 \cdot 10^{-12}\,[31], \end{aligned}$$

which the parameter points are checked against. However, for most of the viable points, this is not a strong constraint since it is mostly fulfilled (in the scalar scenario).

Numerical scans and parameter studies 5

In order to study the parameter-space of the scotogenic minimal model, multiple numerical scans have been conducted. In this chapter, the results are presented and discussed. First, the scalar scenario is investigated in sections 5.1 to 5.3, followed by a scan with fermion Dark Matter. Finally, effects of single parameters are reviewed.

5.1 Scalar scenario random scan

The first parameter scan was conducted for scalar Dark Matter. The method and programs described in chapter 3 were used and the parameters (described in section 2.4) were chosen randomly in their respective intervals for every point. The parameters that span over multiple orders of magnitude (and therefore are mostly studied in logarithmic scale) were created with a distribution yielding a similar amount of points for every order, i.e. a logarithmic distribution. This applies for example to λ_5 in the range from 10^{-12} to 10^{0} and the masses of the fermions $m_{N_i} \in [0.1, 10]$ TeV and the scalar mass input $m_\eta \in ([0.1, 10])$ TeV.
For every point, the masses of the physical particles $m_{\eta^{0R}}$, $m_{\eta^{0I}}$, as well as the fermions m_{N_i} were compared after their random generation, and the fermionic scenarios discarded, leaving the points of the scalar scenario. Every remaining point was then passed on to `SPheno` and `micrOMEGAs` for closer investigation. From this, 452 481 points were successfully obtained with their respective parameters and observables.

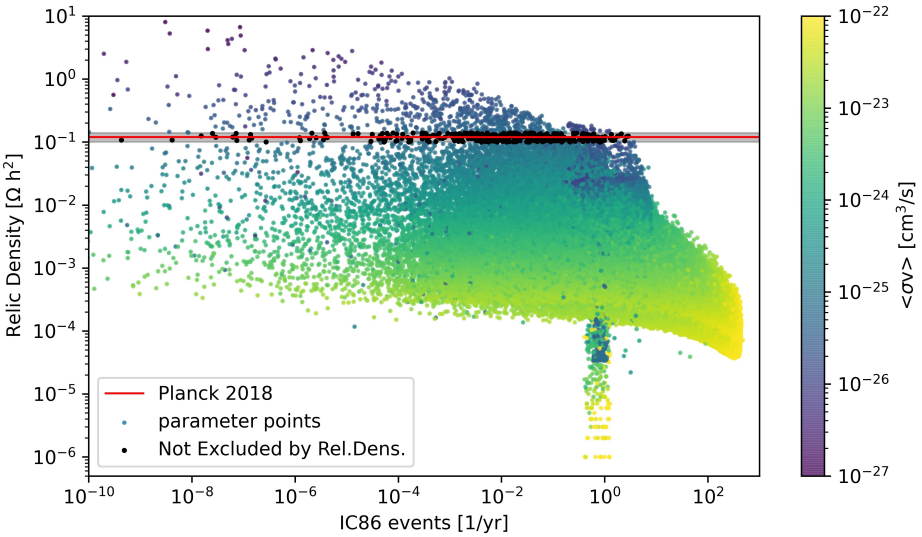

Figure 5.1: Three observables of the points from the *scalar scenario random scan*. The red line marks the result by Planck 2018 [12] with variation of 0.02 marked for better visibility (grey area). The points inside this relic density interval are marked in black. The colour scale denotes the thermal average of the DM annihilation cross-section $\langle \sigma v \rangle$.

Three properties of the investigated parameter points can be seen in fig. 5.1: The relic density, the amount of expected IceCube events per year, as well as the *thermal average annihilation cross-section* $\langle \sigma v \rangle$. This cross-section describes how likely two Dark Matter particles annihilate into Standard Model particles, and combined with

their velocity and averaged, this value is a measure of how much the DM particles annihilate in the universe. The number of IceCube events was determined for each point from the muon (anti-)neutrino fluxes, which were calculated by `micrOMEGAs`. These fluxes (which are energy dependent, see for example fig. 5.7) were then multiplied with their respective effective area of IceCube taken from [32] and integrated over the energy to get the expected number of events (see detailed description in [20]). Most interesting from an experimental viewpoint are the parameter points with the highest possible expected IceCube events (i.e. furthest to the right in the figure) because they would be easier to detect or reject with the experimental data. However, these correspond to smaller relic densities (shown on the y-axis) which would not describe the full amount of Dark Matter corresponding to the experimentally measured value by the Planck telescope. Whilst it is possible that the particles from the scotogenic model only describe parts of Dark Matter, in this work, the focus is laid on the parameter points that describe scenarios in which the scotogenic model accounts for the full Dark Matter relic density. Therefore, the points with high IceCube event rates are excluded by the relic density.
Looking at the distribution of the colours in fig. 5.1, a clear transition from top to bottom can be seen. It shows that the average annihilation cross-section increases for a smaller relic density. This fits to the following logical relation: When more Dark Matter particles annihilate into Standard Model particles in the early universe, the Dark Matter relic density decreases (as a result of a longer equilibrium until freeze-out [19]).
Additionally, a vertical accumulation of parameter points can be seen at around one IceCube event per year. This line consists of points with low DM masses, where the effect of resonances with the Higgs- and Z-boson changes the relic density distinctively. This will be explained further at the end of this section.

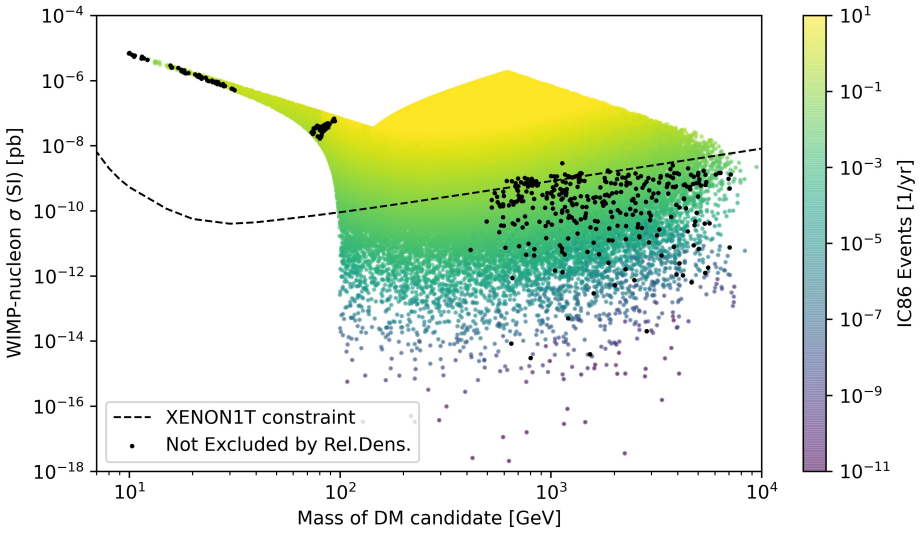

Figure 5.2: Parameter points from the *scalar scenario random scan*. The XENON1T-limit [26] was linearly interpolated and is shown in the region of interest: every parameter point above this line, is to be excluded. The x-axis shows the lightest scalar mass of every point (either $m_{\eta^{0R}}$ or $m_{\eta^{0I}}$), which is the respective DM candidate. Black points have a relic density of $(0.12 \pm 0.02)\,\Omega\,h^2$ and hence fit to the measurement of the Planck telescope [12].

Investigating the WIMP-nucleon scattering cross-section, the points from the parameter scan were compared to the XENON1T-limit, see fig. 5.2. The IceCube experiment also provides a limit for the scattering cross-sections [32]. However, this constraint is currently not as strong as the one provided from the XENON experiment. Therefore, the direct detection limits are used in this work.
The specific shape of fig. 5.2 results from the boundaries of the parameters (e.g. the intervals as listed in section 2.4), and will not be studied further. However, two other essential features can be seen in this figure:
Firstly, the rate of IceCube events (marked by the colour) increases for a higher WIMP-nucleon scattering cross-section. This can be understood in the frame of the processes in the Sun described in section 2.5: More scattering also increases the annihilation rate and hence leads to more detectable neutrinos.
Secondly, two different regions can be made out for the points which result from the relic density constraint (marked in black in fig. 5.2). They can be put into roughly two clusters (for masses smaller and bigger than 200 GeV). The left cluster (with smaller masses) can be fully excluded by the XENON1T limit, while the right cluster is mostly below the experimental limit. Why these two regions are separated so clearly can be seen in fig. 5.3. Here, the connection between the relic density and the Dark Matter mass was plotted. Looking at the points which agree with the experimental value of the relic density (inside the grey area), the two different regions can be found again. In this plot, the points which are additionally not excluded by the XENON1T-limit are marked red and it can be seen that this only includes points in the higher mass region.

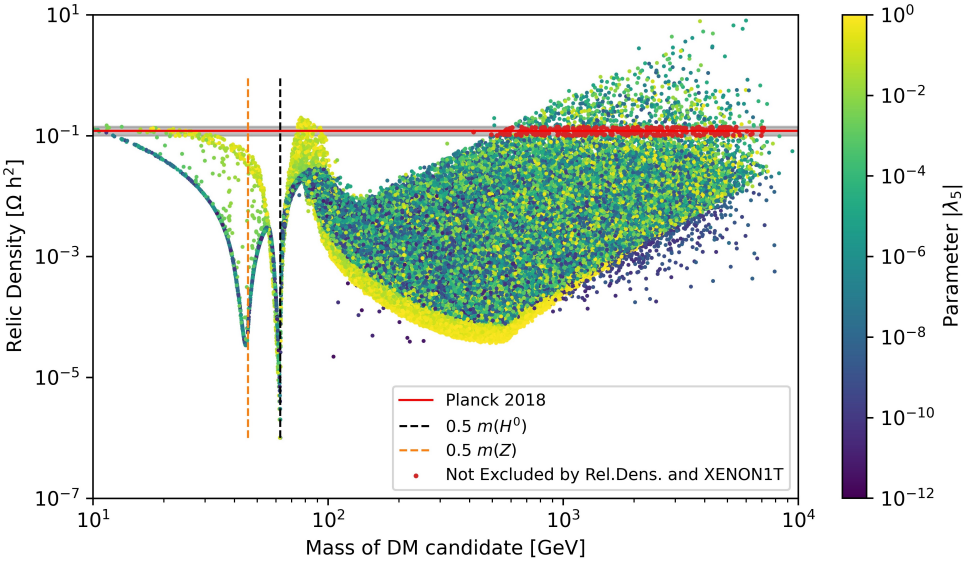

Figure 5.3: Parameter points from the *scalar scenario random scan*. Data of the masses of the Higgs and Z-boson taken from [33]. The x-axis shows the lightest scalar mass for each point (either $m_{\eta^{0R}}$ or $m_{\eta^{0I}}$), which is the mass of the respective DM candidate. In colour, the absolute value of the parameter λ_5 is shown. Note that points with large λ_5 have to be taken with caution because the simulation is optimised for small λ_5 (see section 5.5).

As can be seen in fig. 5.3, for larger DM masses, the points are widely distributed,

whereas for smaller DM masses ($< 200\,\text{GeV}$) the relic density shows a sharper distribution and abrupt changes. This is resulting from the influence of Higgs- and the Z-boson *resonances*. These affect the relic density in the following way: If the WIMP (here η^{0R} or η^{0I}) has half the mass of one of these particles, the annihilation of two WIMPs with one of the bosons becomes very likely (because the mass before and afterwards is the same). Consequently, when more annihilations occur in the early universe, the relic density decreases.
However, the annihilation into a Z-boson is inelastic, and requires the masses of the two scalar particles to be close and therefore this resonance does only affect parameter points with small λ_5 (because λ_5 is directly affecting the mass difference of η^{0R} and η^{0I}). This can be seen in fig. 5.3, where points with larger λ_5 do not follow the Z-resonance.
The difference between the minimum of the Z-resonance (of the parameter points) and the measured Z-mass (added vertical line) attracts attention, but could not be explained. However, the points at the minimum of the resonance show the same annihilation channels and branching ratios as experimentally measured for the Z-boson, hence a Z-resonance with possibly some numerical errors in the simulation process is inferred.
These plots create a clear picture of some basic phenomenology of the scotogenic model in scalar scenarios for some important observables. However, the number of points which are not excluded by all the constraints (XENON1T, relic density) is relatively low compared to the amount of simulated points. In an attempt to increase these viable regions, the effects of coannihilation, first theoretically explained in [34], were studied next (also applied to the scotogenic model in [35]).

5.2 Scalar scenario coannihilation scan

Studying the influence of coannihilations on the observables, in a parameter scan with scalar scenarios, is the aim of this section.
Coannihilations describe the effect of annihilation of two different Dark Matter particles in the early universe. This happens when the masses of the particles are close to each other [35].
In the scotogenic model, coannihilations arise naturally between the scalar particles η^{0R} and η^{0I} for small values of λ_5 (as then the mass difference is small). These lead to a decrease in relic density as it is more likely for the scalar Dark Matter particles to annihilate.
However, coannihilations can not only occur between the two neutral DM scalars, but can also span into the fermion sector. The annihilation cross-section of the fermionic DM particles N_i is mostly determined by the Yukawa couplings which in general can be very small (i.e. annihilation is less likely). Therefore, the relic density increases in a scalar scenario, if one or multiple DM fermions N are coannihilating with the scalar DM candidate [35]. This was implemented in a parameter scan in the way that the masses of the scalar DM particles were sampled first. The lightest scalar mass was then taken and the masses of the three DM fermions set to be only slightly bigger than the mass of the scalar DM particles: $m_{N_1} = m_{N_2} = m_{N_3} = \min(m_{\eta^{0R}}, m_{\eta^{0I}}) + \Delta m$. Δm therefore describes the mass difference between the lightest scalar DM and the DM fermions N_i.
Results from this scan can be seen in fig. 5.4, which shows the relic density against

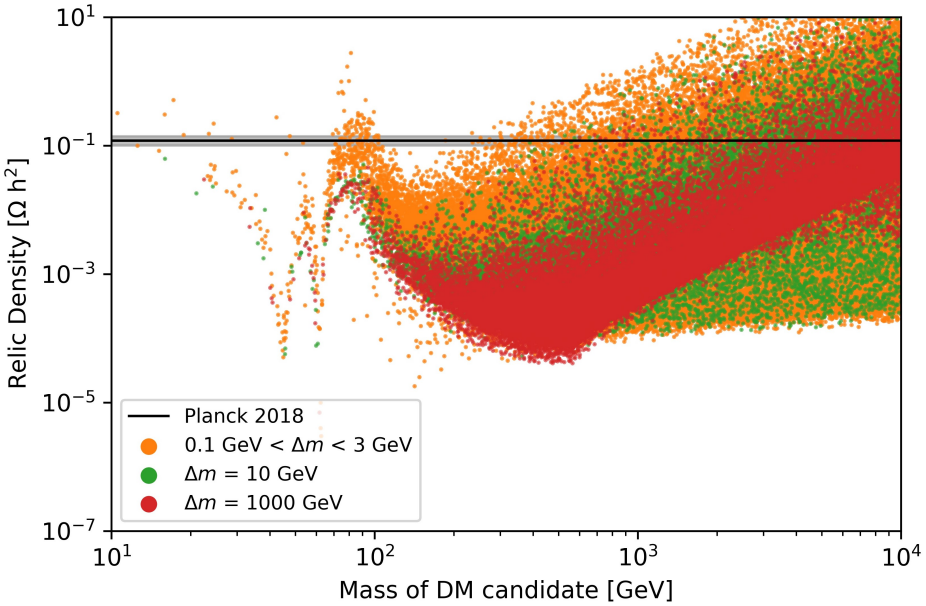

Figure 5.4: Results of a scalar scenario parameter scan: The three fermions N_i were set to have the same mass ($m_{N_1} = m_{N_2} = m_{N_3}$), and the mass difference to the lightest scalar DM particle Δm was chosen to be either 1000 GeV, 10 GeV or in the interval [0.1,3] GeV (randomly sampled). The latter interval promotes coannihilations between the DM fermions N and DM scalars η^{0R} and η^{0I}. This was controlled for some points by looking at the main annihilation channels in the early universe, which are responsible for the relic density.

the mass of the lightest DM particle. In colours, the mass difference Δm between the lightest scalar DM η^{0R} or η^{0I} and lightest fermion DM N_i is marked. The interval $\Delta m \in [0.1, 3]\,\text{GeV}$ was chosen because it is comparably small to the masses of the particles and is roughly in the order of the natural scalar mass splitting. The exact boundaries of the interval are illustrative. However, the precise effect of these boundaries could be subject to further research.

The general shape of the point distribution in fig. 5.4 resembles the previous scan with random masses (fig. 5.3). However, for a small mass difference Δm (orange in fig. 5.4), the points are wider distributed and significantly more points are not excluded by the relic density (i.e. are found in the region $(0.12 \pm 0.02)\,\Omega h^2$). Especially of interest is that the lower mass bound of the region of viable points decreased: Multiple points with the fitting relic density also have smaller masses than in the random scan. This extends the viable parameter-space to lower WIMP masses as described in [35].

The effect that more parameter points induce the experimentally measured value of the relic density can also be seen in fig. 5.5. In this figure, the relic density distribution of three different parameter scans was plotted. The *scalar scenario random scan* (blue) returned many points with a relic density below the measured value. In contrast, the *fermion scenario random scan* (where one or more of the fermion DM particles N_i are the lightest, see section 5.4) resulted in many points with a high relic density (green). Adding coannihilations (orange) between the scalar and fermionic sector increases the amount of viable points at the experimentally measured value from the

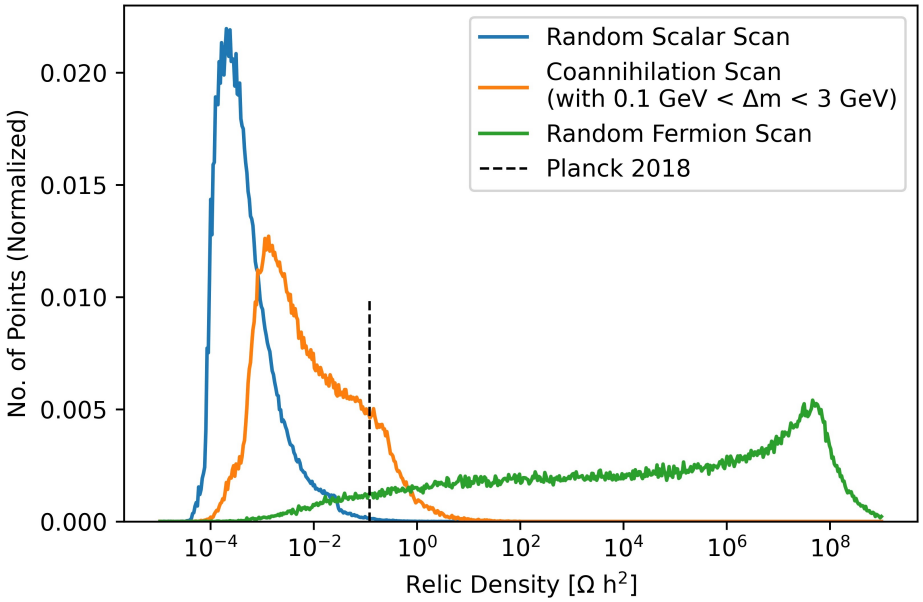

Figure 5.5: Normalised histogram of the relic density of the parameter points from three different parameter-scans: *Scalar random scan* (section 5.1), *scalar coannihilation scan* (section 5.2) and *fermion random scan* (section 5.4). The largest amount of points with the measured relic density are found from the scalar coannihilation scan. Bins of the histogram logarithmically scaled, corresponding to the scaling in this plot.

Planck telescope, and shows a distribution between the scalar and fermion parameter scans.

This has also been found in [35], where the authors additionally study the effect if this coannihilation only happens with one or two fermions. They find that a higher number of fermions participating in the coannihilations also increases the relic density. Thus, the two distributions shown in fig. 5.5 represent the two different ends to this effect (for scalar scenarios), for either no coannihilation (blue) and all three fermions participating coannihilating (orange).

In order to further compare the results of the scalar coannihilation scan to the results obtained earlier in the scalar random scan, fig. 5.6 was generated. It shows the relic density and IceCube events of the points from the scalar coannihilation scan with $\Delta m \in [0.1, 3]\,\text{GeV}$. Here, the shape is comparable to the random scan studied earlier, only with a wider distribution regarding the relic density (which fits to the conclusion that with coannihilations more points with higher relic density are found). The vertical accumulation with low relic densities at around one IceCube event per year is not as distinct as in fig. 5.1, but this is due to the lower number of simulated points (only 182 166 compared to 452 481 in the random scalar scan).

Additionally, the *equilibrium factor* c_{eq} (as defined in section 2.5) is displayed. It can clearly be seen that a state in the Sun close to or at equilibrium ($c_{eq} \to 1$) leads to a higher neutrino flux and therefore a higher rate of possible IceCube events. This effect will be studied and explained further in the following section.

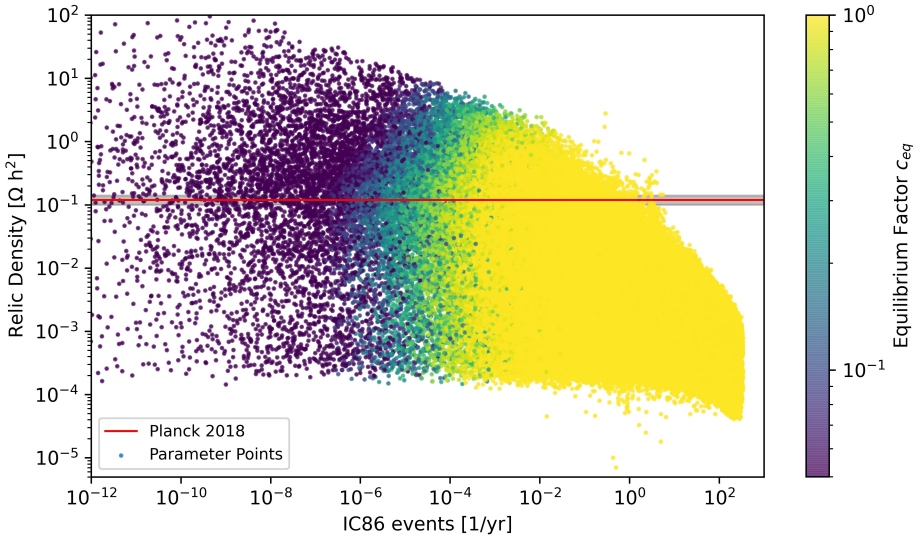

Figure 5.6: Relic density plotted against the (expected) number of IceCube events for points from the *scalar scenario coannihilation scan* ($\Delta m \in [0.1, 3]\,\mathrm{GeV}$). The color encodes the *equilibrium factor* c_{eq} in the Sun, which was introduced in section 2.5: If (very close to) 1, the Sun is in equilibrium, and the number of DM particles being captured in the Sun corresponds to twice the amount of DM to SM particles annihilations happening ($\Gamma_{\chi\chi} = \frac{C_\chi}{2}$).

5.3 Equilibrium studies

In order to study Dark Matter annihilation in the Sun, multiple factors have to be considered. As described in section 2.5, the annihilation rate can be up to half of the capture rate (as two captured Dark Matter particles are always needed to annihilate). However, this is not always the case, because the annihilation rate also depends on the *equilibrium factor* c_{eq}. It takes into account the time of the capturing process and was defined for this work in section 2.5. The importance and effect of this factor can be seen for illustrative purposes in fig. 5.7.

In this figure, a manual calculation assuming equilibrium in the Sun was made and compared to the actual result (which comes from solving the differential equation (2.6)). The large difference spanning many orders of magnitude results from the *equilibrium factor* which is about 10^{-16} at this point. In this case, equilibrium in the Sun would be reached after about 10^{17} years and hence cannot be assumed as a premise.

For further illustration purposes, fig. 5.8 can be considered: This histogram shows the number of points from the scalar coannihilation scan sorted into two categories of either in equilibrium ($c_{eq} > 0.95$) or not ($c_{eq} < 0.95$). The tendency that scalar coannihilation points with higher mass tend to not be in equilibrium can be seen (for elastic scattering in the Sun, which is only implemented in the simulations in this work). This can be explained from multiple aspects that lead to a decrease in the capture rate in the Sun for higher masses [36]: First, for heavier Dark Matter particles, the number density decreases (to have the same relic density), and less scattering and annihilations occur. Additionally, the scattering and capture processes become more difficult because of the larger mass difference of the Dark Matter particles to the light Sun particles, making the minimum scattering energy harder to reach for heavier WIMPs (see [36]).

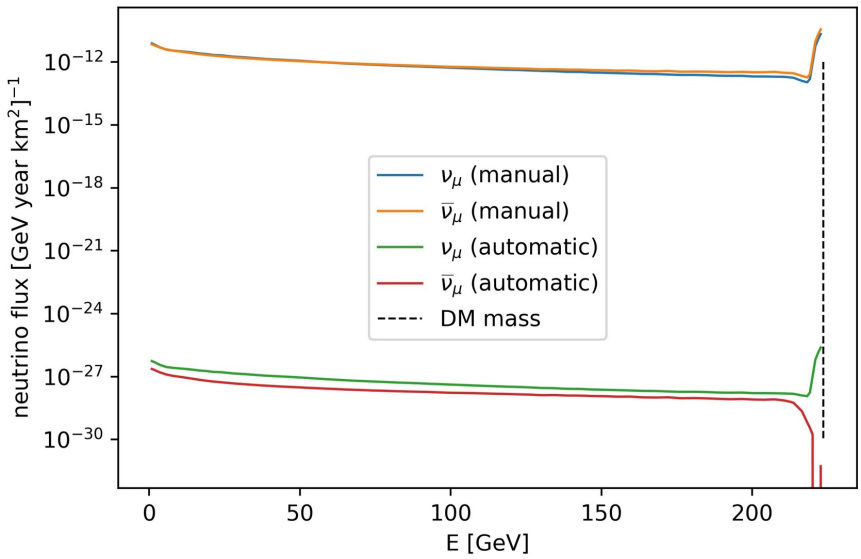

Figure 5.7: Example of the (anti-)muon-neutrino flux from the Sun on Earth at a specific parameter point, which is a scalar scenario described as *BS2* in Vicente [37] (*page 29 following*). The automatic flux was calculated directly from the `micrOMEGAs` function `neutrinoFlux()`, which accounts for the *equilibrium factor* in eq. (2.8). The manual calculation was done using the function `basicNuSpectra()` for the largest channels neglecting the equilibrium factor (assuming the Sun is always in equilibrium). The resonance for neutrinos close to the DM mass can be seen in both fluxes because this point includes direct annihilation channels of the scalar DM particles into SM neutrinos.

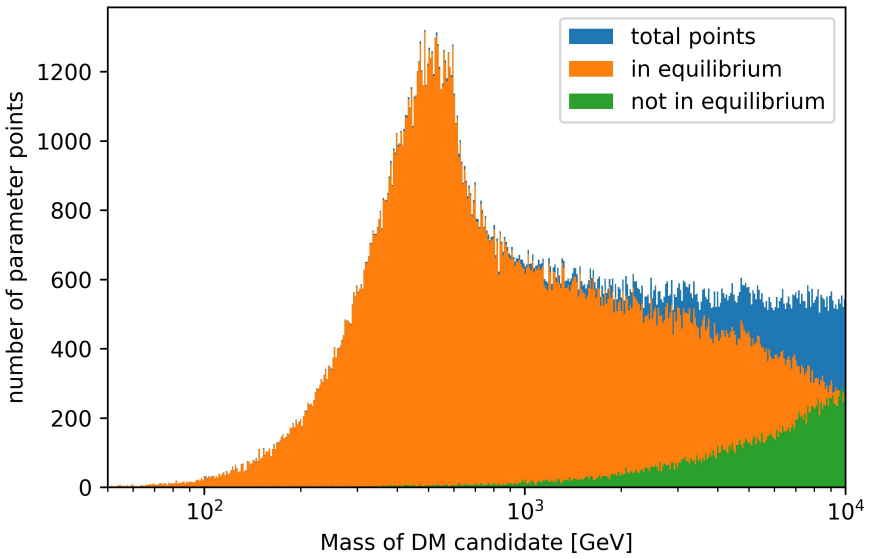

Figure 5.8: Histogram of parameter points from the *scalar coannihilation scan* for illustration purposes. The cutoff in the equilibrium factor was chosen to be 0.95 ($c_{eq} > 0.95$ means already in equilibrium, for $c_{eq} < 0.95$, the Sun has not yet reached equilibrium).

Therefore, equilibrium calculations should be kept in mind for the scotogenic model, especially for heavy Dark Matter particles.
In order to have a full picture of the scotogenic model and its observables, fermion scenarios will be studied in the following section.

5.4 Fermion scenario scans

In the fermionic scenario in the scotogenic model, one of the fermions N_i is the lightest Dark Matter particle constituting the DM candidate. In this case, no scattering with Standard Model particles (i.e. no XENON1T signal), and therefore also no neutrino flux from the Sun (i.e. no IceCube signals) is expected. This comes from the fact that the DM fermions don't couple to the SM Higgs boson (in the new Lagrangian). Because of the absence of these constraints, two others are considered here: Lepton flavour violation processes and the relic density (as described in chapter 4). Lepton flavour violation processes have not been studied in detail for scalar scenarios, as they only exclude small parts of the parameter-space compared to the direct and indirect detection constraints.
A large parameter scan was conducted, similar to the *scalar scenario random scan* (see section 5.1), except that here only the cases in which one of the DM fermions N_i has the smallest mass were simulated. The λ-parameters were randomly sampled in their intervals for every point.

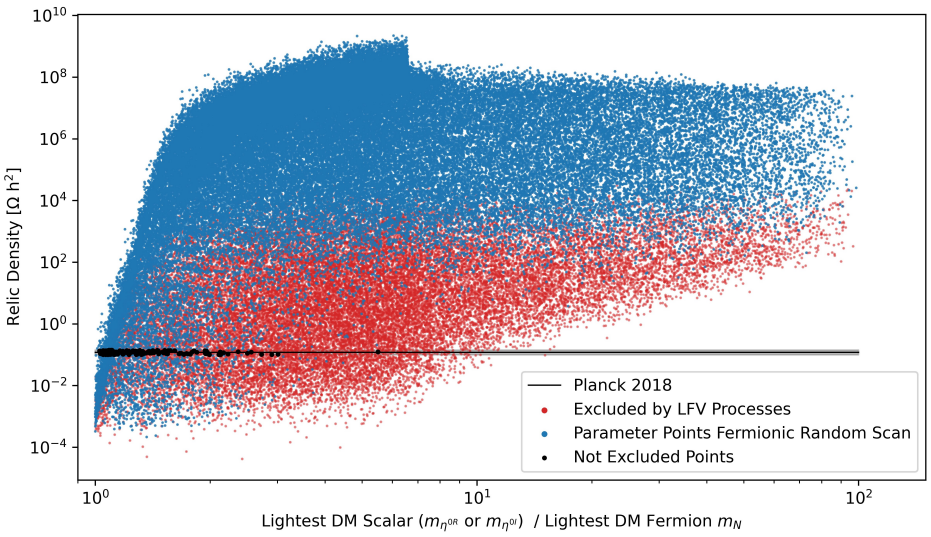

Figure 5.9: Parameter points of the *fermion scenario random scan*, plotted with their relic density against the ratio of the lightest DM scalar to the lightest DM fermion. Red points are excluded by the experimental limits of lepton flavour violation (LFV) as listed in chapter 4. The considered processes are $\mu \to e\gamma$, $\mu \to 3e$, Conversion$(\mu - e, \mathrm{Ti})$), as suggested in [15] with limits from [29]–[31].
Black marked points are not excluded by LFV and the relic density constraint.

First, to study the constraints of lepton flavour violation, fig. 5.9 was plotted. It shows the relic density against the ratio of the lightest scalar DM to the lightest fermion DM.

Here, it can be seen the general trend that a large ratio (i.e. a larger mass difference Δm) leads to larger relic densities. This shows that in a mostly fermionic scenario with suppressed coannihilations, the relic density is significantly higher than the actual experimental value. In contrast to this, for a small mass ratio, the coannihilation effects lead to a smaller relic density, which can comply to the measurements. Additionally, the lepton flavour violation constraint also excludes the points with smaller relic densities and larger ratios (marked in red). Therefore, the most viable points are found for small mass ratios between the lightest DM scalar and the lightest DM fermion (< 2). The effect that LFV can restrict a large area of points in a random fermion scan was also found and studied in detail in [38].
Because most viable points were found at a smaller ratio between the lightest particles of the scalar and fermionic DM, the influence of coannihilations in a fermionic scenario was further investigated. Three additional scans were carried out looking at the consequence of the same masses for the three fermions ($m_{N_1} = m_{N_2} = m_{N_3}$), as well as enforced coannihilations with the scalar sector. The relic density distributions of these scans are displayed and compared in fig. 5.10.

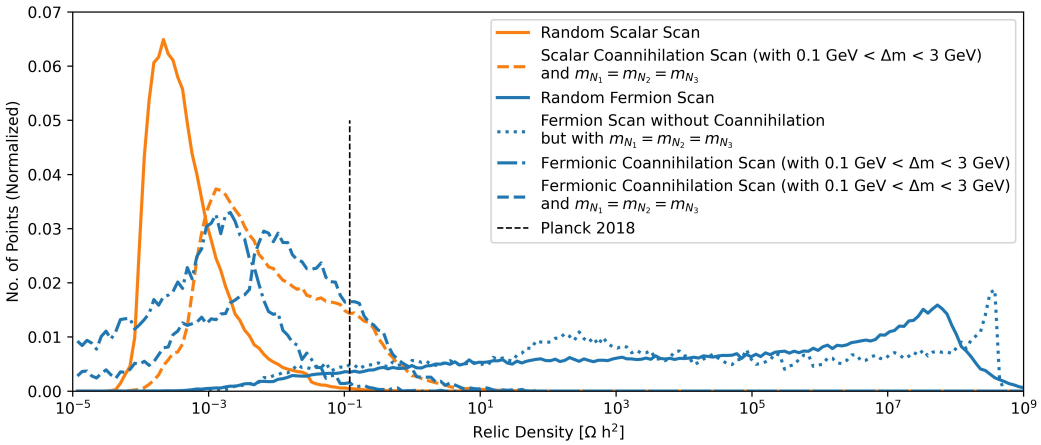

Figure 5.10: Histograms of the relic density of different parameter scans, normalised by respective number of simulated points. In orange, a scalar particle η^{0R} or η^{0I} is the lightest DM particle. For blue distributions, a fermion particle N_1, N_2 or N_3 is DM candidate. Bins of the histogram are logarithmic, according to the scaling of the figure. It can be seen that in both cases (scalar and fermion), the coannihilation scan with all three fermions at the same mass yield the most points in the viable region.

In this figure, it can be observed that the number of coannihilating DM fermions also plays a role (see different blue distributions): If only one Dark Matter fermion is included (dashed-dotted line), many points are found with a relic density even lower than measurements. This means that the viable region of the scotogenic model (if accounting for all the Dark Matter) for a fermionic scenario is maximised with all the fermions at the same mass, and additional coannihilating scalar particles.
Overall, in fig. 5.10, a stark contrast between the scalar scan with random masses for all the Dark Matter particles, and the same with a fermionic scan can be made out. This can be explained with the different annihilation cross-sections: As the DM fermions N_i have a considerably smaller annihilation cross-section (because of the Yukawa instead

of the SM Higgs coupling [35]), less Dark Matter particles would have annihilated in the early universe, which results in a very high relic density. Whereas the scalar DM particles η come with a high annihilation cross-section, and hence predominantly have a smaller relic density. A combination of these annihilation cross-sections via enforcing coannihilations thus leads to more parameter points in the viable region around 0.12 Ωh^2, as can be seen in fig. 5.10. This works for scalar as well as for fermionic DM in the scotogenic model.
All of the parameter scans so far were carried out to investigate the impacts of the mass-parameters of the Dark Matter particles. In the following section, effects of the λ-parameters will be studied individually.

5.5 Single parameter studies

For the purpose of studying the influence of the parameters λ_3, λ_4, λ_5 as well as the scalar Dark Matter mass ($m_{\eta^0 I}$ or $m_{\eta^0 R}$) individually, the parameter scans described in this section were performed. The scans were conducted on the basis of an initial point, called BS1 (*benchmark scotogenic 1*). This point was found in the *scalar scenario coannihilation scan* (section 5.2) and results in a relic density of $0.115\,\Omega\mathrm{h}^2$. Additionally, it is not excluded by the XENON1T-limit and lepton flavour violation experiments. The point BS1 has the following (relevant) mass and λ-parameters:

$$\begin{aligned}
\lambda_1 = 0.26, \lambda_2 = 0.5, \lambda_3 = 0.8810, \lambda_4 = -1.0117, \lambda_5 = 0.0028 \\
m_{\eta^+} = 568.5580\,\mathrm{GeV}, m_{\eta^{0R}} = 540.9965\,\mathrm{GeV}, m_{\eta^{0I}} = 540.8384\,\mathrm{GeV} \\
m_{N_1} = m_{N_2} = m_{N_3} = 542.5755\,\mathrm{GeV} \\
\Delta m = 1.7370\,\mathrm{GeV}
\end{aligned}$$

As described earlier, Δm is defined as the mass difference between the lightest particles of the fermion and scalar sector. In this point, it is relatively small which leads to coannihilations between the two Dark Matter sectors. Furthermore, λ_5 is large enough ($> 10^{-4}$) to provide a big enough mass splitting of η^0 to be in the region where inelastic scattering in the Sun can be neglected ($m_{\eta^{0R}} - m_{\eta^{0I}}$ larger than several hundred keV [36]).
In these parameter scans, λ_3, λ_4, λ_5 and the mass $m_{\eta^{0I}}$ were individually varied in their intervals (as listed in section 2.4). While changing the individual λ-parameters, the input parameter for the scalar mass m_η^2 was accordingly adjusted so that the physical mass $m_{\eta^{0I}}$ (which also depends on the λ-parameters, see eq. (2.5) in section 2.3) stayed the same and therefore all points still have the same DM candidate mass (except for the λ_5-scan, see below). Additionally, Δm was also chosen to stay constant during all the scans in this section. Note that this approach is mostly of qualitative nature because the parameters are interconnected and the starting point is defining the behaviour significantly (especially in the case of λ_5, see below).
During the parameter scans, only the parameters listed above remained fixed, while the parameters which are implemented in the simulation (such as neutrino masses and Yukawa coupling) are free within their boundaries (see section 2.4). This can lead to multiple points that are called *BS1*. However, these points only show very small variations, which are neglected.
Two observables of all single parameter scans together are displayed in fig. 5.11.

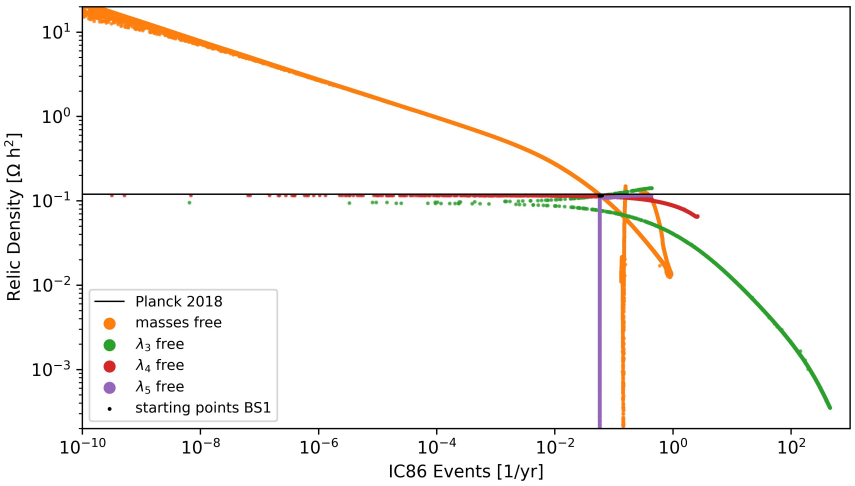

Figure 5.11: Single parameter scans based on the benchmark point parameters BS1. Different scans marked with different colors. Yukawa matrix and neutrino parameters still randomly sampled as described in section 2.4, therefore multiple points BS1 are plotted. Planck result value for the relic density from [12].

Figure 5.11 clearly shows the individual effect of the parameters on the relic density as well as the IceCube events: Whereas λ_4 mostly affects the number of IceCube events (red), but not the relic density, λ_5 predominantly changes the latter (purple). The scalar Dark Matter mass and λ_3 here show a behaviour of altering both observables at the same time (orange and green). The unsteady shape of the parameter scan with varied particle masses is a direct result from a resonance with the Higgs boson that can be seen in fig. 5.12.

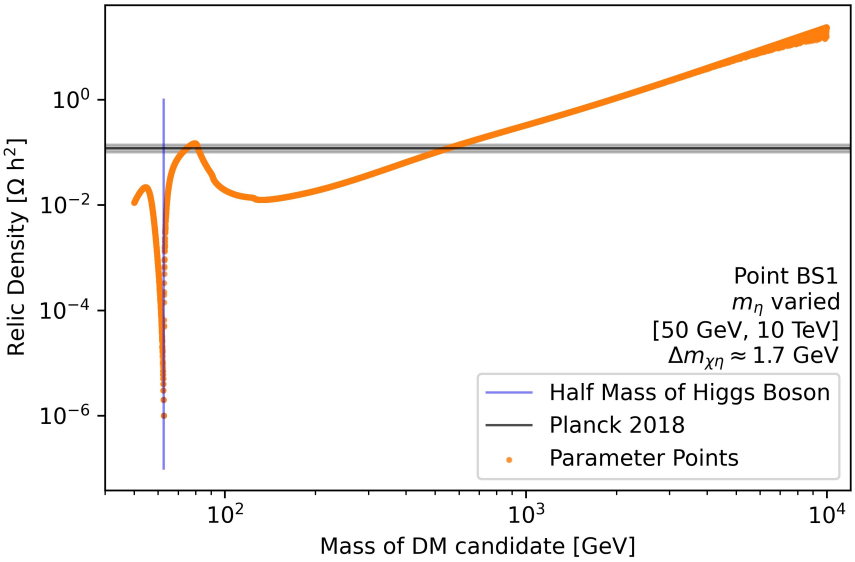

Figure 5.12: Parameter Scan with mass of scalar DM candidate $m_{\eta^{0I}}$ changed (by changing the input m_η^2, see eq. (2.5)). As the mass difference Δm is set to be constant ($\Delta m = 1.7370\,\text{GeV}$), the fermion masses also change accordingly.

The different scans are analysed individually in further detail, beginning with the scan with varied Dark Matter particle mass. Figure 5.12 shows a similar behaviour to earlier scalar parameter scans (random or coannihilation). The relic density increases for points with higher masses, which is expected considering that the particle density stays the same. Furthermore, for Dark Matter candidate masses around half the mass of the Higgs boson, a resonance can be observed.

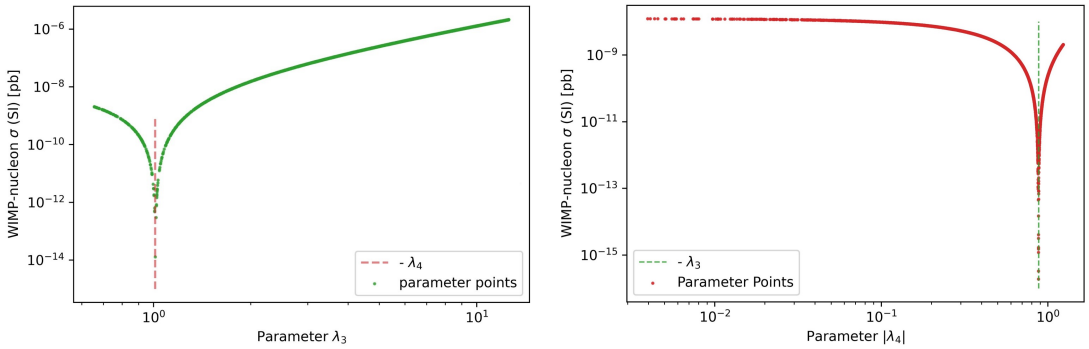

Figure 5.13: Single parameter scans of λ_3 (left) and λ_4 (right) with the other λ-parameters and masses as in point BS1. Here, the WIMP-nucleon spin-independent cross-section is plotted against the parameters and the negative of the other parameter is added as vertical line.

Studying the parameters λ_3 and λ_4, resonances in their scattering cross-sections with SM particles can be found (see fig. 5.13). These correspond to the cases when $\lambda_3 + \lambda_4 \approx 0$: Neglecting λ_5 (which is comparably small), the coupling of η to the Higgs boson in the potential in the Lagrangian (eq. (2.2)) approaches zero for this condition, which therefore reduces the scattering drastically. This leads to less annihilations in the Sun, which in turn provide less measurable neutrinos in the IceCube experiment.

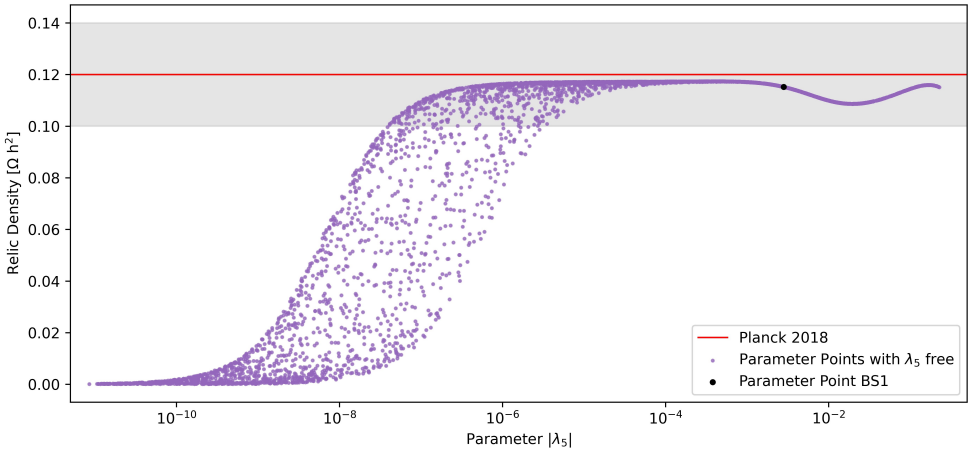

Figure 5.14: Parameter scan with varying λ_5-parameter. The other λ-parameters, as well as the masses are fixed over the course of the scan. Results for large $|\lambda_5|$ have to be considered with care.

The last investigated parameter λ_5 shows a more complex behaviour, see fig. 5.14. In

this figure, the relic density is plotted against λ_5. As the distribution is symmetrical around zero, the absolute value is used. The parameter was sampled for every point with a logarithmic distribution in the interval $\pm[10^{-12}, \lambda_3 + \lambda_4 + \sqrt{\lambda_1 \lambda_2}]$. Recall that due to the Casas-Ibarra implementation, the Yukawa-matrix is large for small λ_5 (see section 2.4). With a large Yukawa-coupling, coannihilations with the Dark Matter fermions N_i are more likely and hence actually lower the relic density significantly. This can explain the small relic density for λ_5 close to zero.
With larger $|\lambda_5|$, the relic density increases until it is mostly only determined by scalar Dark Matter processes in the early universe (because BS1 is a scalar scenario). This marks the upper limit of the relic density in the figure. The parameter λ_5 should in general be small because lepton flavour is conserved in the limit $\lambda_5 \to 0$ [39], and since lepton flavour violation has not been measured yet, it can only be very rare (i.e. λ_5 should be small). Therefore, the parameter points with higher λ_5 than the starting point have to be considered with caution. The full behaviour which can be seen for larger λ_5 in fig. 5.14 is not understood in this work. It might be influenced by a SM Higgs resonance in the early universe as well as a smaller coupling for $\lambda_3 + \lambda_4 + \lambda_5 = 0$. The shape of fig. 5.14 is also influenced by the fact, that BS1 has coannihilations between the scalar and fermion Dark Matter particles and shows a different behaviour for large $|\lambda_5|$ for other starting points. This could be subject for further studies in the future.
The single parameter scans underline the importance of the consideration of all parameters of a single point, and the influences on the observables relic density and IceCube events could be investigated.

Summary

6

This work studied various aspects of the scotogenic minimal model [13]. The model provides a solution for the neutrino mass problem of the Standard Model and could also account for the Dark Matter mass. In the frame of the scotogenic model, the physical Dark Matter particle is WIMP Dark Matter and either one of the neutral scalar particles (η^{0R} or η^{0I}), or the lightest of the three fermions (N_i). Furthermore, only elastic scattering was implemented in the simulation.

6.1 Discussion

As described in chapter 5, multiple parameter scans were performed and studied. This numerical analysis is often done in order to understand the possibilities and the potential of Dark Matter models (for example in [15], [20], [35], [40]). The overall aim of the scans presented here was to present fundamental aspects and phenomena of the scotogenic minimal model.
As this whole work is based on ideas and concepts of modern Dark Matter research, it is fully of theoretical nature, which makes a detailed discussion of uncertainties inexpedient. The focus is instead laid on qualitative descriptions. However, as for example seen for the Z-resonance in fig. 5.3, numerical errors can undoubtedly play an important role.
Studying the outcome of the parameter scan, the intrinsic constraints of the parameter scans have to be kept in mind, which for example here include neutrino hierarchy and neutrino mass limits. As there are various experiments ongoing which are trying to determine these boundaries further (for example the KATRIN experiment), the parameter-space probably will be even further constrained in the future.
Regarding the constraints from observables, the following aspects were found. Firstly, the relic density was understood for different scans. The experimentally measured value of $\Omega h^2 = 0.12$ is setting a strong constraint: In all the parameter scans conducted in this work, only a small amount of points were found close to the experimental value (e.g. see fig. 5.1). To maximise the amount of viable parameter points around this value, coannihilations were introduced and their effect studied. The largest amount of viable parameter points was found for coannihilation scans with all new DM particles involved (scalar and fermionic). This is the case for scalar as well as fermion Dark Matter candidates and can be seen clearly in fig. 5.10.
Additionally, as the Dark Matter particles of the scotogenic model could also account for only part of the actual relic density, parameter points with a relic density smaller than 0.12 should not be discarded. This is especially true for the scalar scenario scans, where many points fall into this category.
Secondly, the XENON1T constraint (as for example shown in fig. 5.2) can only be applied for scalar dark matter in the scotogenic model. Here, it mostly excludes viable points with low masses ($< 100\,\mathrm{GeV}$) which unfortunately also would have provided higher IceCube event rates.
Considering the IceCube experiment, the scalar coannihilation scan showed the highest event rates for the viable points. But even in this case, the expected numbers of measurable events were found to be very low (on the order of a few events per year). However, in this work only elastic scattering in the Sun was considered. Taking inelastic scattering into account could make this mode of searching for hints of this model

interesting again. This can be done by including other programs into the tool-chain, which is performed in the recent paper [20].
Finally, for the scalar scenarios, lepton flavour violation processes did not pose a strong constraint on the points which were not already excluded either by relic density or XENON1T. However, for fermion DM, this constraint rules out many of the points in a random scan without coannihilations with scalar DM particles (which was also found in [38]). This results from the need of comparably high Yukawa couplings in order to reach the measured relic density. Therefore, more LFV is found, which leads to more excluded points [41]. If coannihilation is added, more points are left in the fermionic scan, but these in their turn still remain undetectable to XENON1T and IceCube (see chapter 4).

6.2 Outlook

Big parts of the parameter-space of the scotogenic model are already excluded. This has been found in various papers (e.g. [15], [38]), and was also confirmed in the scans that were conducted in this work.
This is the case especially for the fermionic dark matter scenario, in which lepton flavour violations pose a big constraint. In the scalar parameter scans, with the points excluded by the relic density and XENON1T, the remaining points are very hard to detect with IceCube and other neutrino telescopes. However, with further improvements to the XENON-experiment, more still viable points come in reach for a possible signal or exclusion (see fig. 5.2).
In further scans, including inelastic scattering in the calculations can lead to higher IceCube events, which could make this model interesting for neutrino telescopes again (see recent paper [20]).
Additional constraints from experiments such as LEP, LHC, or studying neutrino fluxes from the DM Halo of the Milky Way, could also be considered in further studies of the scotogenic model.
Another interesting aspect for future works could be to investigate the specific effect of the parameter λ_5 on the model in further detail. Furthermore, the single parameter scans could be investigated and compared to other scans with regards to the starting point.
Overall, the scotogenic model still can't fully be ruled out, as many parameter points still remain viable. Especially its simplicity and phenomenology are persuasive enough to keep this model in mind for further studies. Other models similar to this are already being studied (see recent overview in [14]), and if future experiments (e.g. XENONnT, DARWIN, IceCube Upgrade) possibly detect a signal, this theoretical research could hopefully be of great use.

Bibliography

[1] D. Galbraith, *Ux: Standard model of the standard model*, Accessed on the 16-03-2021. [Online]. Available: `http://davidgalbraith.org/portfolio/ux-standard-model-of-the-standard-model/`.

[2] G. Aad *et al.*, 'Observation of a new particle in the search for the standard model higgs boson with the atlas detector at the lhc,' *Physics Letters B*, vol. 716, no. 1, pp. 1–29, Sep. 2012. arXiv: `1207.7214v2`.

[3] J. Woithe, G. J. Wiener and F. V. der Veken, 'Let's have a coffee with the standard model of particle physics!' *Physics Education*, vol. 52, no. 3, p. 034 001, Mar. 2017.

[4] C. L. Cowan, F. Reines, F. B. Harrison, H. W. Kruse and A. D. McGuire, 'Detection of the free neutrino: A confirmation,' *Science*, vol. 124, no. 3212, pp. 103–104, 1956.

[5] G. Danby *et al.*, 'Observation of high-energy neutrino reactions and the existence of two kinds of neutrinos,' *Physical Review Letters*, vol. 9, pp. 36–44, 1962.

[6] K. Kodama *et al.*, 'Observation of tau neutrino interactions,' *Phys. Lett. B*, vol. 504, pp. 218–224, 2001. eprint: `hep-ex/0012035`.

[7] L. Oberauer and J. Oberauer, *Neutrinophysik*, ger, 1st ed. 2019. Springer Spektrum, 2019.

[8] R. H. Sanders, *The Dark Matter Problem: A Historical Perspective*. Cambridge University Press, 2010, ch. 2.

[9] F. Zwicky, 'Die Rotverschiebung von extragalaktischen Nebeln,' *Helvetica Physica Acta*, vol. 6, II 1933.

[10] S. Profumo, *An Introduction to Particle Dark Matter*. World Scientific Publishing Europe Ltd., 2017.

[11] J. P. Hughes, 'The Mass of the Coma Cluster: Combined X-Ray and Optical Results,' *The Astrophysical Journal*, vol. 337, p. 21, Feb. 1989.

[12] Planck-Collaboration, 'Planck 2018 results. vi. cosmological parameters,' 2020. arXiv: `1807.06209`.

[13] E. Ma, 'Verifiable radiative seesaw mechanism of neutrino mass and dark matter,' *Physical Review D*, vol. 73, no. 7, Apr. 2006. arXiv: `hep-ph/0601225`.

[14] S. May, 'Minimal dark matter models with radiative neutrino masses: From lagrangians to observables,' M.S. thesis, WWU, Münster, Germany, Jun. 2018. arXiv: `2003.04157`.

[15] T. de Boer, M. Klasen, C. Rodenbeck and S. Zeinstra, 'Absolute neutrino mass as the missing link to the dark sector,' *Physical Review D*, vol. 102, no. 5, Sep. 2020. arXiv: 2007.05338v2.

[16] I. Esteban, M. C. Gonzalez-Garcia, A. Hernandez-Cabezudo, M. Maltoni and T. Schwetz, 'Global analysis of three-flavour neutrino oscillations: synergies and tensions in the determination of θ_{23}, δ_{CP}, and the mass ordering,' *JHEP*, vol. 01, p. 106, 2019. arXiv: 1811.05487.

[17] J. Casas and A. Ibarra, 'Oscillating neutrinos and $\mu \to e,\gamma$,' *Nuclear Physics B*, vol. 618, no. 1-2, pp. 171–204, Dec. 2001. arXiv: hep-ph/0103065.

[18] M. C. Gonzalez-Garcia, M. Maltoni, J. Salvado and T. Schwetz, 'Global fit to three neutrino mixing: Critical look at present precision,' *Journal of High Energy Physics*, Dec. 2012. arXiv: 1209.3023v3.

[19] E. W. Kolb, *Fine-Tuning in the Physical Universe*. Cambridge University Press, 2020, ch. 9. DOI: 10.1017/9781108614023.

[20] T. de Boer, R. Busse, A. Kappes, M. Klasen and S. Zeinstra, 'Indirect detection constraints on the scotogenic dark matter model,' May 2021. arXiv: 2105.04899.

[21] G. Bélanger, J. Da Silva, T. Perrillat-Bottonet and A. Pukhov, 'Limits on dark matter proton scattering from neutrino telescopes using micrOMEGAs,' *JCAP*, vol. 12, p. 036, 2015. arXiv: 1507.07987.

[22] A. Gould, 'Resonant Enhancements in WIMP Capture by the Earth,' *Astrophys. J.*, vol. 321, p. 571, 1987.

[23] F. Staub, 'SARAH 4 : A tool for (not only SUSY) model builders,' *Comput. Phys. Commun.*, vol. 185, pp. 1773–1790, 2014. arXiv: 1309.7223.

[24] W. Porod and F. Staub, 'SPheno 3.1: Extensions including flavour, CP-phases and models beyond the MSSM,' *Comput. Phys. Commun.*, vol. 183, pp. 2458–2469, 2012. arXiv: 1104.1573.

[25] D. Barducci, G. Belanger, J. Bernon, F. Boudjema and J. Da Silva, *Micromegas: The user's manual, version 5.0*, Feb. 2019. [Online]. Available: https://lapth.cnrs.fr/micromegas/v5.0/manual_5.0.pdf.

[26] E. Aprile *et al.*, 'Dark Matter Search Results from a One Ton-Year Exposure of XENON1T,' *Phys. Rev. Lett.*, vol. 121, no. 11, p. 111 302, 2018. arXiv: 1805.12562.

[27] E. Aprile *et al.*, 'Projected WIMP sensitivity of the XENONnT dark matter experiment,' *JCAP*, vol. 11, p. 031, 2020. arXiv: 2007.08796.

[28] Wikipedia, *Icecube neutrino observatory*, https://en.wikipedia.org/wiki/IceCube_Neutrino_Observatory, Accessed on the 03-05-2021.

[29] A. M. Baldini *et al.*, 'Search for the lepton flavour violating decay $\mu^+ \to e^+\gamma$ with the full dataset of the MEG experiment,' *Eur. Phys. J. C*, vol. 76, no. 8, p. 434, 2016. arXiv: 1605.05081.

[30] U. Bellgardt *et al.*, 'Search for the Decay $\mu^+ \to e^+ e^+ e^-$,' *Nucl. Phys. B*, vol. 299, pp. 1–6, 1988.

[31] C. Dohmen *et al.*, 'Test of lepton flavor conservation in mu → e conversion on titanium,' *Phys. Lett. B*, vol. 317, pp. 631–636, 1993.

[32] M. G. Aartsen *et al.*, 'Search for annihilating dark matter in the Sun with 3 years of IceCube data,' *Eur. Phys. J. C*, vol. 77, no. 3, p. 146, 2017, [Erratum: Eur.Phys.J.C 79, 214 (2019)]. arXiv: 1612.05949.

[33] P. Zyla *et al.*, 'Review of Particle Physics,' *PTEP*, vol. 2020, no. 8, p. 083C01, 2020. DOI: 10.1093/ptep/ptaa104.

[34] K. Griest and D. Seckel, 'Three exceptions in the calculation of relic abundances,' *Phys. Rev. D*, vol. 43, pp. 3191–3203, 1991.

[35] M. Klasen, C. E. Yaguna, J. D. Ruiz-Alvarez, D. Restrepo and O. Zapata, 'Scalar dark matter and fermion coannihilations in the radiative seesaw model,' *JCAP*, vol. 04, p. 044, 2013. arXiv: 1302.5298.

[36] A. Menon, R. Morris, A. Pierce and N. Weiner, 'Capture and Indirect Detection of Inelastic Dark Matter,' *Phys. Rev. D*, vol. 82, p. 015 011, 2010. arXiv: 0905.1847.

[37] A. Vicente, 'Computer tools in particle physics,' Jul. 2015. arXiv: 1507.06349.

[38] A. Vicente and C. E. Yaguna, 'Probing the scotogenic model with lepton flavor violating processes,' *JHEP*, vol. 02, p. 144, 2015. arXiv: 1412.2545.

[39] J. Kubo, E. Ma and D. Suematsu, 'Cold Dark Matter, Radiative Neutrino Mass, $\mu \to e\gamma$, and Neutrinoless Double Beta Decay,' *Phys. Lett. B*, vol. 642, pp. 18–23, 2006. arXiv: hep-ph/0604114.

[40] J. Fiaschi, M. Klasen, M. Vargas, C. Weinheimer and S. Zeinstra, 'MeV neutrino dark matter: Relic density, lepton flavour violation and electron recoil,' *JHEP*, vol. 11, p. 129, 2019. arXiv: 1908.09882.

[41] T. Toma and A. Vicente, 'Lepton Flavor Violation in the Scotogenic Model,' *JHEP*, vol. 01, p. 160, 2014. arXiv: 1312.2840.

Acknowledgments

I would like to express my gratitude to everyone who helped me making this work possible.

First of all to *Prof. Dr. Alexander Kappes* for giving me the opportunity to join his group to start my journey into Dark Matter physics, and his support for my future studies.

To the best supervisor *Raffaela Busse* for explaining the whole topic to me, guiding me and keeping me busy, as well as answering all my questions and giving important and valuable comments to my drafts multiple times.

To *Prof. Dr. Christian Weinheimer* for being second examiner and supporting me on my path in the future.

To *Thede de Boer* for a very helpful discussion and *Martin Unland* for providing essential feedback.

To the whole working group for a very welcoming atmosphere.

And last but not least to Meghan for the best English support, Anni for the wonderful layout template and my friends and family for being interested and supporting me throughout this whole time.

Declaration of Academic Integrity

I hereby confirm that this thesis on *Parameter-space studies of Dark Matter annihilation in the Sun in the scotogenic minimal model* is solely my own work and that I have used no sources or aids other than the ones stated. All passages in my thesis for which other sources, including electronic media, have been used, be it direct quotes or content references, have been acknowledged as such and the sources cited.

01.06.2021 Jim Kopka

I agree to have my thesis checked in order to rule out potential similarities with other works and to have my thesis stored in a database for this purpose.

01.06.2021 Jim Kopka